Nonsense-Mediated Decay as the Molecular Cause for Autosomal Recessive Bestrophinopathy in Two Unrelated Families

Esther Pomares,[1,2,3] *Anniken Burés-Jelstrup,*[4] *Sheila Ruiz-Nogales,*[1,2,3] *Borja Corcóstegui,*[4] *Roser González-Duarte,*[1,2,3] *and Rafael Navarro*[4]

Purpose. To characterize the molecular basis of two novel *BEST1* mutations causing autosomal recessive bestrophinopathy (ARB). Strong evidence argues in favor of the dominant negative effects of most autosomal dominantly inherited mutations, whereas there is only weak support for the molecular basis of the ARB phenotype.

Methods. Patients underwent ophthalmic examination, color and autofluorescence fundus imaging, optical coherence tomography (OCT), electrooculogram, and full-field electroretinogram (ERG). *BEST1* was directly screened for mutations in two ARB unrelated patients. The pathogenicity of the new *BEST1* variants was assessed in silico and in vivo.

Results. Two unrelated patients with diagnoses of ARB showed retinal pigment epithelial disturbances and abnormal ERGs. Each patient was homozygous for a novel *BEST1* mutation, c.521_522del and c.1100+1G>A. A carrier sibling (WT/c.521_522del) was unaffected. Both mutations generate a frameshift and a premature stop codon that, if translated, would seriously compromise bestrophin-1 function. However, the in vivo quantitative RT-PCR assays showed that most of the mutated transcripts were eliminated before translation because the mRNA-*BEST1* levels were dramatically diminished the controls.

Conclusions. In truncating *BEST1* mutations, the null phenotype associated with ARB is attributed to a substantial decrease of *BEST1* expression promoted by the nonsense-mediated decay (NMD) surveillance mechanism. Moreover, the severity of the phenotype increases with the preserved amount of altered transcript, suggesting that the clinical outcome reflects the combined null and dominant negative effects of the two mutations over the patient's genetic background. (*Invest Ophthalmol Vis Sci.* 2012;53:532–537) DOI:10.1167/iovs.11-7964

Autosomal recessive bestrophinopathy (ARB) is a recently reported retinal disorder caused by mutations in *BEST1*,[1] a gene known to be associated with a variety of degenerative eye disorders, among them Best vitelliform macular dystrophy (BVMD), adult-onset foveomacular vitelliform dystrophy, and other clinical entities causing widespread ocular abnormalities such as autosomic dominant vitreoretinochoroidopathy (ADVIRC) and autosomic dominant MRCS (microcornea, rod-cone dystrophy, early-onset cataract, and posterior staphyloma) syndrome.[2] *BEST1* encodes an integral transmembrane protein of 585 amino acids that localizes mainly to the basolateral membrane of the retinal pigment epithelium (RPE).[3] The bestrophin-1 protein functions as a Ca^{2+}-activated Cl^- channel, a regulator of voltage-gated Ca^{2+} channels, a volume-regulated Cl^- channel, and an HCO_3^- channel. Although its precise physiological role is still unknown, bestrophin-1 dysfunction has been associated with defective regulation of the subretinal fluid reabsorption and with aberrant phagocytosis of the photoreceptor disks.[4]

ARB is characterized by varying RPE defects that predominantly affect the posterior pole but that can extend beyond the vascular arcades. Unlike BVMD, vitelliform deposits in the macular area are an uncommon finding, whereas yellowish subretinal deposits or, more typically, small, punctate, white subretinal deposits surrounding the macular area are a frequent trait. Moreover, other clinical features, such as hyperopia, shallow anterior chamber, and high incidence of angle-closure glaucoma, are shared by ARB-affected persons, denoting common traits with other *BEST1*-related diseases such as ADVIRC syndrome.[1]

At present, more than 150 dominant mutations in *BEST1*-causing BVMD have been identified. In contrast, only 10 recessive variants are known to cause ARB.[1,5,6] The high degree of variability in the clinical features and the different inheritance patterns of the *BEST1* mutations have prompted functional studies[7] from which novel genotype-phenotype correlations are emerging: though nonfunctional bestrophin-1 (null phenotype) has been associated with recessive ARB, most dominantly inherited missense mutations produce dominant negative effects.[2] Interestingly, in vitro functional studies have shown that seven recently reported missense recessive mutants abolish correct trafficking, promote early degradation, or induce aggresome-like inclusion bodies of bestrophin-1, causing the ARB disease phenotype.[7] However, the real molecular impact of the *BEST1* nonsense mutations is still unclear. Here we describe two ARB patients who have homozygous truncating mutations and show that the levels of mRNA *BEST1* are, in both cases, greatly compromised because of the nonsense-mediated decay (NMD) surveillance mechanism.

Patients and Methods

Patients

Two unrelated patients from Spanish families were diagnosed with ARB. One was from consanguineous origin and had two unaffected

From the [1]Departament de Genètica, Facultat de Biologia, and the [2]Institut de Biomedicina, Universitat de Barcelona, Barcelona, Spain; [3]Centro de Investigación Biomédica en Red de Enfermedades Raras (CIBERER), Instituto de Salud Carlos III, Barcelona, Spain; and [4]Instituto de Microcirugía Ocular, Barcelona, Spain.

Supported in part by Grants SAF2009-08079 (Ministerio de Ciencia e Innovación) and SGR2009-1427 (Generalitat de Catalunya), CIBERER (U718), and ONCE (RG-D). EP and SR were under contract by CIBERER.

Submitted for publication May 31, 2011; revised October 13 and December 3, 2011; accepted December 10, 2011.

Disclosure: **E. Pomares**, None; **A. Burés-Jelstrup**, None; **S. Ruiz-Nogales**, None; **B. Corcóstegui**, None; **R. González-Duarte**, None; **R. Navarro**, None

Corresponding author: Rafael Navarro, Instituto de Microcirugía Ocular, C. Josep Maria LLadó 3, 08035 Barcelona, Spain; navarro@imo.es.

siblings, and the second was an isolated proband whose family history was not available. Informed consent from the patients and relatives was obtained, following the tenets of the Declaration of Helsinki. All work concerning patient recruitment and sample collection had been approved by the Bioethics Committee of the University of Barcelona (Barcelona, Spain). DNA was obtained from blood samples (MoleStrips DNA Blood Kit with the GeneMole instrument; Mole Genetics, Mole, Lysaker, Norway).

Clinical Examination

Clinical examination of the affected patients included best-corrected visual acuity (BCVA) testing using standard Snellen charts, intraocular pressure measurement, slit lamp biomicroscopy, and funduscopy. Patients also underwent color fundus and autofluorescence imaging (Topcon TRC-50IX IMAGEnet and Spaide AF Filters; Topcon Corporation, Tokyo, Japan). Optical coherence tomography (OCT) was obtained for both patients (Cirrus HD-OCT; Carl Zeiss Meditec Inc., Dublin, CA). Full-field electroretinogram (ERG) and electrooculogram (EOG) were performed in both affected patients according to the International Society for Clinical Electrophysiology of Vision (ISCEV) Standards.[8,9] Both sisters of one of the patients underwent clinical examination, which included color and autofluorescence retinography, OCT examination, and EOG.

Mutational Screening of *BEST1*

All 11 exons and exon-intron boundaries of the *BEST1* gene were directly screened for mutations. Genomic DNA of patients was amplified using specific primers (Supplementary Table S1, http://www.iovs.org/lookup/suppl/doi:10.1167/iovs.11-7964/-/DCSupplemental) and sequenced (BigDye version 3.1 kit [Applied Biosystems, Inc. [ABI], Foster City, CA] in the ABI PRISM 3730 DNA sequencer [Applied Biosystems, Inc.]).

Bioinformatic Analysis

All sequences were analyzed using sequence assembly software (Seqman; DNAStar, Madison, WI) and were aligned with the genomic wild-type *BEST1* sequence (NM_004183) from the public database UCSC Genome Browser (http://genome.ucsc.edu/, provided in the public domain by UCSC Genome Bioinformatics, University of California at Santa Cruz, Santa Cruz, CA).

Splicing site score values of the wild-type and variant sequences of *BEST1* were predicted online at SplicePort (http://spliceport.cs.umd.edu/, provided in the public domain by the University of Maryland,

Figure 1. Fundus imaging and OCT of affected patients and one sibling. (**A**–**F**) Patient 48.1. Fundus retinography of the right (**A**) and left (**B**) eyes depicting characteristic ARB findings in both eyes: diffuse RPE irregularity at the posterior pole and around the optic disc and small, punctate, white subretinal deposits in the macular area (*black arrows*). OCTs of right (**C**) and left (**D**) eyes show neurosensorial macular thinning with subretinal and intraretinal fluid. Autofluorescence retinography of right (**E**) and left (**F**) eyes elucidates diffuse and more extensive RPE disturbances than those seen with the conventional retinography (*arrowheads*). (**G**–**L**) Subject 48.2. Color retinography (**G**, **H**) shows normal fundus with no RPE disturbances. OCTs (**I**, **J**) are normal, with no intraretinal or subretinal fluid, and autofluorescence retinography findings (**K**, **L**) are normal in both eyes. (**M**–**R**) Patient 64.1. Fundus retinography of right (**M**) and left (**N**) eyes shows multifocal, irregular vitelliform subretinal deposits at the posterior pole of both eyes (*arrowheads*). Small, punctate, subretinal flecks are also present in the macular area (*arrows*). OCTs of right (**O**) and left (**P**) eyes show subretinal fluid. Intraretinal cysts are present in both eyes but are more marked in the right eye. Left eye OCT shows subretinal material deposition (*white arrowheads*). Autofluorescence retinography of right (**Q**) and left (**R**) eyes depicts irregular vitelliform material deposition (*black arrowheads*) and RPE disturbances that primarily affect the posterior pole (*black arrows*).

College Park, MD), Geneid (http://genome.imim.es/genepredictions/index.html, provided in the public domain by the Genome Bioinformatics Research Laboratory, Center for Genomic Regulation, Spanish Bioinformatics Institute, Barcelona, Spain), and BDGP (http://www.fruitfly.org/, provided in the public domain by the Berkeley Drosophila Genome Project, University of California at Berkeley).

RT-PCR Analysis of *BEST1* Expression

Blood total RNA was obtained (RiboPure-Blood; Ambion, Austin, TX) from patients, relatives, and an unrelated control subject. To avoid RNA degradation, samples were mixed with RNA stabilizer (RNALater; Ambion) in a 1:4 ratio after blood collection. Total RNA was retrotranscribed (Transcriptor High-Fidelity cDNA Synthesis Kit; Roche Applied Science, Indianapolis, IN) with random hexamers and oligo(dT)18 in accordance with the manufacturer's instructions. Amplification of transcripts from *BEST1* and *GAPDH* (used as control) was accomplished using specific primers from different exons (Supplementary Table S1, http://www.iovs.org/lookup/suppl/doi:10.1167/iovs.11-7964/-/DCSupplemental). PCR was performed in a final volume of 50 μL, using the GoTaq Flexi DNA polymerase (Promega, Madison, WI) under three different sets of conditions. For amplification of *GAPDH*, three-step PCR was performed as follows: denaturation for 2 minutes at 94°C, followed by 35 cycles of 20 seconds at 94°C, 30 seconds at 63°C, and 1 minute at 72°C. For amplification of *BEST1*, two different conditions were used. First, for amplification of exons 8 to 10, three-step PCR was performed: denaturation for 2 minutes at 94°C, followed by 35 cycles of 20 seconds at 94°C, 30 seconds at 60°C, and 50 seconds at 72°C. Second, for amplification of exons 8 to 11, three-step PCR was performed: denaturation for 2 minutes at 94°C, followed by 35 cycles of 20 seconds at 94°C, 30 seconds at 60°C, and 75 seconds at 72°C. RT-PCR products were resolved by electrophoresis and semiquantitated with image acquisition and analysis software (Quantity One 4.5; Bio-Rad, Hercules, CA). Values were normalized against *GAPDH* levels and were represented as a ratio of *BEST1/GAPDH*. The control wild-type ratio *BEST1/GAPDH* was arbitrarily set at 100%.

Real-time RT-PCR assay was performed with SYBR Green Master mix (LightCycler 480 SYBR Green I Master; Roche Applied Science, Indianapolis, IN) using specific primers for *BEST1* (exons 10 and 11) (Supplementary Table S1, http://www.iovs.org/lookup/suppl/doi:10.1167/iovs.11-7964/-/DCSupplemental). *HPRT* was used as control. For each real-time RT-PCR reaction, 2 μL cDNA template, 1 μM each primer, 1× master mix, and 1 μL water were mixed in a final volume of 10 μL. The reaction was set at 45 cycles in a two-step program: 94°C for 20 seconds and 56°C for 30 seconds. For each sample, four replicates with their corresponding negative controls were assayed. Transcript expression was quantified by using the second-derivative maximum method (LightCycler 480, version 1.5.0; Roche Applied Science). Values were normalized against *HPRT* levels and represented as a ratio of *BEST1/HPRT*. The wild-type ratio *BEST1/HPRT* was arbitrarily set at 100%.

Results

Clinical Findings

Patient 48.1, a 42-year-old man, was referred to our institution because of bilateral low visual acuity since infancy, with marked worsening during the past 2 years. His medical history was significant for bacterial meningitis at the age of 2 years and severe plaque psoriasis for which he had previously received treatment with topical and oral steroids, PUVA therapy, methotrexate, and efalizumab. Current treatment for his psoriasis at the time of the visit was periodical subcutaneous injections of etanercept only. The patient was of Spanish origin; his parents were first cousins, and he had two unaffected sisters, subjects 48.2 and 48.3.

At the time of the visit, the patient's BCVA was 20/100 OD and 20/200 OS. Anterior segment examination results were normal in both eyes, revealing a deep anterior chamber bilat-

Table 1. Clinical Characteristics of Patients 48.1 and 64.1 and the Carrier Sibling 48.2

Patient or Carrier	Sex	Age at Onset (y)	Age at Examination (y)	Visual Acuity	Fundus Findings	OCT Findings	Full-Field ERG	EOG (OD/OS)	Mutation
48.1	Male	37	42	OD 20/100, OS 20/200	Widespread RPE irregularity affecting posterior pole and toward equator, small pale subretinal deposits in the macular area	Subretinal and intraretinal fluid	Delayed and reduced rod and cone ERG	Reduced/Reduced	c.521_522/c.521_522del
48.2	Female	—	40	OD 20/20, OS 20/20	Normal OU	Normal OU	Normal OU	Normal/Normal	c.521_522del/wt
64.1	Male	8	17	OD 20/100, OS 20/40	Widespread RPE disturbances, small pale subretinal deposits in the macula. Large, multiple yellowish subretinal deposits affecting the posterior pole	Subretinal and intraretinal fluid Subretinal deposits	Reduced amplitudes of both cones and rods	Normal/Normal	c.1100+1G>A/c.1100+1G>A

erally. Fundus examination revealed diffuse RPE irregularity throughout the posterior fundus, around the optic disc, and in the temporal quadrant with small, punctate, pale subretinal deposits in the macular area, slight vascular attenuation, and peripapillary vascular sheathing. These findings were confirmed by autofluorescence retinography, which revealed RPE alteration throughout the posterior pole, more severe RPE disturbances in the macular area, and a concentric area of hyperautofluorescence extending from the optic disc. OCT imaging showed discrete subfoveal fluid in both eyes and small intraretinal cysts (Figs. 1A–F). EOG showed a reduced light rise in both eyes and a pathologic Arden index of 100 OD and 110 OS. Full-field ERG showed reduction and delay of both cone and rod function in both eyes, with lower amplitudes in the left eye (Table 1). Given these clinical and electrophysiological findings, bestrophinopathy was suspected.

The two unaffected siblings of the patient (subjects 48.2 and 48.3) underwent complete ophthalmologic examination, including retinography, fundus autofluorescence, OCT, and electrophysiological testing. OCT and autofluorescence results were normal in both sisters, who had no signs of RPE disturbance or subfoveal fluid (Figs. 1G–L). Full-field ERG and EOG were within normal limits in both sisters.

Patient 64.1, a 17-year-old boy, was referred to our institution because of bilateral progressive visual loss and a diagnosis, made at another institution, of bilateral macular edema of unknown origin. His medical history was significant for moderate developmental delay and bilateral hypoacusis. The patient was of Spanish origin and had been adopted, so no information was available about his biological progenitors. At the time of the visit, the patient's BCVA was 20/100 OD and 20/40 OS. Anterior segment examination results were normal in both eyes. The most striking finding in the fundus examination was the presence of a well-demarcated yellowish subretinal deposit surrounding the fovea in both eyes, with multiple punctate and small subretinal deposits scattered throughout the posterior pole. These findings were confirmed by autofluorescence retinography, which revealed multiple hyperautofluorescent lesions at the posterior pole corresponding to the yellowish subretinal deposits and consistent with multiple vitelliform deposits. The optic nerve was normal. OCT imaging showed intraretinal cysts and subfoveal fluid in both eyes, together with subretinal material deposition (Figs. 1M–R). Full-field ERG revealed reduced amplitudes affecting both cones and rods. EOG was within normal limits, with an Arden index of 180 in both eyes (Table 1). The clinical picture, though phenotypically different from that of the first case, made us suspect bestrophinopathy.

Molecular Findings

Sequencing all the exons of *BEST1* in patient 48.1 identified a homozygous two-nucleotide deletion in exon 5, c.521_522del (p.Leu174Glnfs*57) (Supplementary Fig. S1A, http://www.iovs.org/lookup/suppl/doi:10.1167/iovs.11-7964/-/DCSupplemental). This deletion resulted in a frameshift from codon 174 and led to a premature stop codon after the addition of 56 amino acids. The proband's asymptomatic sisters were subsequently analyzed. One of them (48.3) had two wild-type alleles, whereas the other (48.2) was heterozygous for the c.521_522del mutation.

Patient 64.1 was found to harbor a homozygous nucleotide substitution, c.1100+1G>A, in the first position of intron 9 embedded in the highly conserved GT donor splice site (Supplementary Fig. S1B, http://www.iovs.org/lookup/suppl/doi:10.1167/iovs.11-7964/-/DCSupplemental).

In Silico Analysis

To assess the pathogenicity of the c.1100+1G>A mutation of patient 64.1, three different splicing prediction algorithms—SplicePort, Geneid, and BDGP—were used. They all predicted that the variant sequence abolished the recognition of the intron 9 donor site and that aberrant splicing would ensue. To gain insight into the expression pattern of this mutated *BEST1* allele, new experiments were set up.

Expression and Splicing Pattern Analyses of *BEST1* Mutations

The c.521_522del variant located in exon 5 caused a frameshift that resulted in a premature stop codon in the mature mRNA. It has been shown that transcripts harboring premature termination codons are detected by the mRNA quality control system and eliminated before translation by NMD.[10] To assess whether the c.521_522del mutation had an effect on the transcription products, we performed semiquantitative RT-PCR analysis in the white blood cell mRNA of patient 48.1, the carrier sibling 48.2, and a wild-type control (Fig. 2A). The results clearly showed a dramatic decrease in patient 48.1 and a detectable reduction in the heterozygous nonaffected sibling (48.2) of the *BEST1* transcripts.

The second variant, c.1100+1G>A, affected the first position of intron 9 of *BEST1*. Because in silico predictions supported a severe effect in the splicing pattern, the expression products of *BEST1* in the white blood cells of patient 64.1 were analyzed. After sequencing several RT-PCR products, consistent evidence in favor of exon 9 skipping were gathered (Fig. 3). Moreover, the new splicing pattern generated a frameshift that resulted in a premature termination codon after the addition of 32 amino acids, p.Val317Profs*. We assumed that the altered transcript could be degraded by NMD. In agreement with this hypothesis, the RT-PCR semiquantification assay showed a severe reduction of the mutated transcript compared with the control (Fig. 2B). To evaluate the decrease in transcriptional products in the affected patients and the nonaffected carrier, a real-time RT-PCR assay was devised. In accordance with the semiquantitative tests, a severe reduction of *BEST1* transcripts was observed for patient 48.1 (13%), the carrier sibling 48.2 (63%), and patient 64.1 (22%) compared with a wild-type control

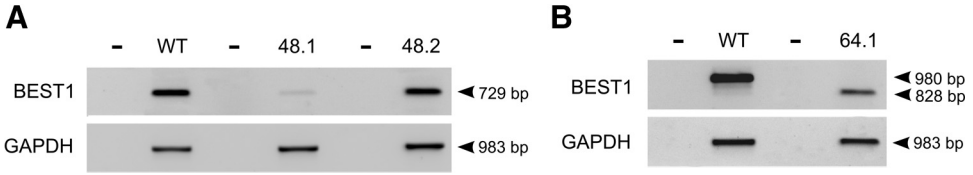

FIGURE 2. *BEST1* RT-PCR analysis in white blood cell mRNA from the patients, a carrier sibling, and a control. (**A**) Patient 48.1 showed a dramatic decrease of the *BEST1* transcript, whereas there was only a moderate reduction in the nonaffected heterozygous sibling 48.2. (**B**) Patient 64.1, bearing the homozygous mutation c.1100+1G>A, showed an aberrantly spliced *BEST1* transcript (828 bp) at a decreased level compared with the control (980 bp).

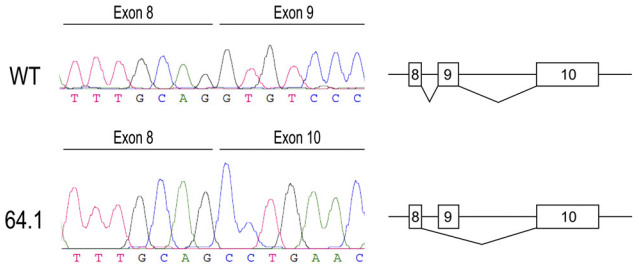

Figure 3. *BEST1* mRNA sequence from a control subject and patient 64.1. Sequences of the two RT-PCR bands from exons 8 to 11 (as shown in Fig. 2B) were unequivocally assigned, 980 bp to the expected wild-type product and 828 bp to the aberrant transcript skipping exon 9, in patient 64.1.

(100%) (Fig. 4). The consistency of the transcriptional levels was shown by an independent RT-PCR assay using more upstream primers, in exons 3 and 4, and no differences in the amounts of the *BEST1* transcripts were detected (data not shown). Overall, our data suggested that the NMD quality control mechanism was responsible for both disease phenotypes.

Discussion

The molecular analyses of *BEST1* mutations highlight distinct pathogenic disease mechanisms underlying bestrophinopathy and depict complex relationships between the phenotypes observed for BVMD and ARB and the molecular defects. The genotype-phenotype correlations are relevant for the proper functional characterization of the mutations, help to establish an accurate prognosis, and are crucial to approach gene replacement therapies. Although most mutations associated with BVMD are missense mutations that do not compromise protein synthesis, the few ARB-causing mutations reported to date are premature truncations or missense substitutions that lead to early transcript degradation or nonfunctional proteins and are associated with a null-phenotype. Although the recessive nature of seven ARB missense mutants has been recently shown in transiently transfected HEK293 cells,[7] no molecular evidence is available for the truncated isoforms. Our data support mRNA degradation by the NMD mechanism in two ARB mutants that generate a premature stop codon, c.521_522del and c.1100+1G>A. Indeed, recent evidence supports that NMD degradation depends, at least in some disease-causing genes, on the position of the premature translation termination codons (PTCs). In these cases, the severity of the clinical manifestations correlates with the abundance of the PTCs, which increases in upstream truncating mutations.[11] Thus, in patient 48.1, the premature stop codon is in position 230, and only 13% of the *BEST1* transcripts are preserved, whereas in patient 64.1, with a stop codon in position, preservation amounts to 22%. Interestingly, we also show that *BEST1* expression is not restricted to the RPE[1] but is also detected in white blood cells, which favors in vivo quantitation of the mRNA-*BEST1* levels in patients and controls.

The differences encountered in the molecular analysis of *BEST1* mutations in both patients allow us to make some phenotypic comparisons and to correlate the clinical expression with the genetic findings. Although patient 48.1 has a characteristic ARB phenotype, patient 64.1 shows ophthalmologic features attributed to both ARB and BVMD.

Patient 48.1 shows the typical bestrophin-1 null-phenotype attributed to the almost total absence of bestrophin-1 in the molecular analysis. The absence of vitelliform material, widespread RPE alterations affecting the posterior pole and progressing beyond the vascular arcades, intraretinal and subretinal fluid in the OCT, and abnormal EOG and ERG are consistent with the clinical findings described previously in ARB.[1] It is also interesting that the carrier sister (subject 48.2), with approximately half the number of normal *BEST1*-mRNA levels, shows a totally normal fundus with no electrophysiological abnormalities. Given this finding, we can conclude that, in the absence of an allele causing a negative dominant effect, 50% of the wild-type bestrophin-1 warrants RPE normal functioning and produces a wild-type phenotype.

Patient 64.1 shows some clinical differences from patient 48.1, even though they both bear autosomic recessive *BEST1* truncating homozygous mutations. The fundus shows multiple, irregular subretinal deposits of vitelliform material that are more characteristic of a multifocal BVMD. However, these deposits are irregular, affect both the macular and the extramacular areas, and are associated with more widespread RPE alterations and intraretinal fluid in the OCT, which are highly unusual in BVMD and are more consistent with ARB. The phenotypic differences encountered in this patient, compared with the typical null-phenotype, may be explained by the different truncation pattern of bestrophin-1. The null-phenotype is easily explained because the mutation produces an early truncation of the protein, and presumably no bestrophin-1 is available in the RPE. On the other hand, patient 64.1 bears a homozygous mutation that generates a more delayed truncation, produces 22% of the *BEST1* transcripts, and en-

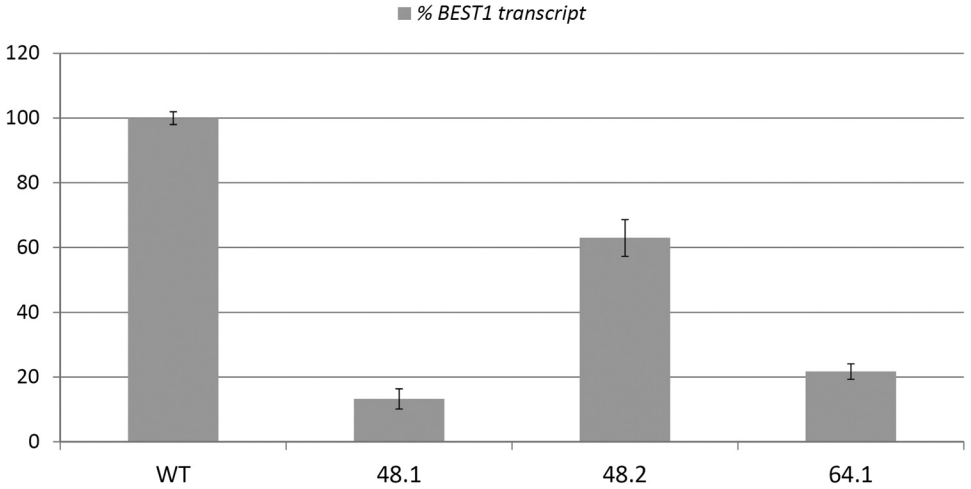

Figure 4. Quantification of the *BEST1* transcripts by real-time RT-PCR in a wild-type subject, patients 48.1 and 64.1, and carrier sibling 48.2. The wild-type subject was considered the control (100%). Note that patient 48.1 had a dramatic decrease in *BEST1* transcript levels (13%), whereas carrier sibling 48.2 produced approximately 63% of the transcripts. Patient 64.1 also showed a severe reduction (22%) of the *BEST1* transcripts.

codes an aberrant protein. Because of the molecular and clinical findings, we cannot consider this patient to have a pure null-phenotype. The clinical picture is more consistent with ARB but shares some common traits with BVMD, with vitelliform deposits the more typical finding.

The age difference between the two patients is also relevant regarding the different phenotypes. Vitelliform material tends to disappear with age and is replaced by progressive RPE atrophy. Although little information about the ophthalmic history of patient 48.1 was available, earlier examinations never mentioned vitelliform lesions or clinical findings other than unspecific RPE disturbances and, lately, macular edema. Hence, we cannot confirm whether this subject's past phenotype has shared similarities with the phenotype of patient 64.1. Moreover, patient (64.1) had hypoacusia and developmental delay, which, to our knowledge, has not been reported in the literature in association with *BEST1* mutations. Another disconcerting feature in patient 64.1 is the normal EOG in both eyes, described in BVMD[12–14] but not in ARB. Part of the explanation could be that the EOG light response is not, or is not only, generated by bestrophin-1.[15] However, a molecular basis for the EOG light response is still missing. Moreover, the severity of the clinical picture in several forms of BVMD has been linked to specific mutations in highly conserved regions of the protein.[16] These severe subtypes also show a typically abolished EOG, in contrast to other less severe forms, in which EOG is reduced but not abolished. Because patient 64.1 shows a phenotype with combined ARB and BVMD traits, we hypothesize that this could partially explain the normal EOG of the proband 64.1.

Both patients bore a similar genetic defect, a homozygous frame-shifting *BEST1* mutation that causes NMD. However, they differed at the clinical and electrophysiological level, probably because of the location of the mutation and their different genetic backgrounds. Whereas proband 48.1 bore a mutation resulting in a premature stop codon that severely compromises bestrophin-1 synthesis, proband 64.1 presented a more downstream mutation that could preserve some protein product. This residual amount of aberrant protein could promote a negative effect, causing the mixed phenotype described with both ARB and BVMD traits.

Recently, a rare recessive inheritance pattern of BVMD was reported in two patients bearing a homozygous single nucleotide deletion in *BEST1*.[17] Genetically, these cases could be classified as ARB, contrary to the BVMD phenotypes. However, the reported mutation (c.1415delT) caused a premature stop codon in a downstream position near the end of the transcript. In this case, consistent with our data, only residual NMD degradation could be assumed. The very terminal position of this mutation could explain that, in homozygosity, a considerable fraction of aberrant transcripts is maintained and causes a negative effect leading to a BVMD-like phenotype. In heterozygosity, as is the case of the nonaffected parents, the wild-type allele produces enough wild-type protein to counterbalance the negative effect of the preserved fraction of the mutant transcripts. The present work unveils the increasing complexity of phenotypes resulting from *BEST1* mutations. Remarkably, proband 48.1, with only 13% of *BEST1* transcripts, would show the expected true null phenotype.

Finally, the spectrum of *BEST1* phenotypes is extremely varied and will continue to increase in complexity as new mutations appear. Genetic testing and molecular analysis will shed light on the emerging genotype-phenotype correlations, promote the understanding of the phenotypic variability in *BEST1*-related pathologies, and open new avenues to clarify the role of this gene in ocular development and retinal physiology.

Acknowledgments

The authors thank the members of the two families for their participation in this study.

References

1. Burgess R, Millar ID, Leroy BP, et al. Biallelic mutation of BEST1 causes a distinct retinopathy in humans. *Am J Hum Genet.* 2008; 82:19–31.
2. Boon CJ, Klevering BJ, Leroy BP, Hoyng CB, Keunen JE, den Hollander AI. The spectrum of ocular phenotypes caused by mutations in the BEST1 gene. *Prog Retin Eye Res.* 2009;28:187–205.
3. Petrukhin K, Koisti MJ, Bakall B, et al. Identification of the gene responsible for Best macular dystrophy. *Nat Genet.* 1998;19:241–247.
4. Xiao Q, Hartzell HC, Yu K. Bestrophins and retinopathies. *Pflugers Arch.* 2010;460:559–569.
5. Gerth C, Zawadzki RJ, Werner JS, Heon E. Detailed analysis of retinal function and morphology in a patient with autosomal recessive bestrophinopathy (ARB). *Doc Ophthalmol.* 2009;118:239–246.
6. Davidson AE, Sergouniotis PI, Burgess-Mullan R, et al. A synonymous codon variant in two patients with autosomal recessive bestrophinopathy alters in vitro splicing of BEST1. *Mol Vis.* 2011; 16:2916–2922.
7. Davidson AE, Millar ID, Burgess-Mullan R, et al. Functional characterisation of bestrophin-1 missense mutations associated with autosomal recessive bestrophinopathy (ARB). *Invest Ophthalmol Vis Sci.* 2011;52:3730–3736.
8. Marmor MF, Fulton AB, Holder GE, Miyake Y, Brigell M, Bach M. ISCEV Standard for full-field clinical electroretinography (2008 update). *Doc Ophthalmol.* 2009;118:69–77.
9. Marmor MF, Brigell MG, McCulloch DL, Westall CA, Bach M. ISCEV standard for clinical electro-oculography (2010 update). *Doc Ophthalmol.* 2011;122:1–7.
10. Hentze MW, Kulozik AE. A perfect message: RNA surveillance and nonsense-mediated decay. *Cell.* 1999;96:307–310.
11. Nicholson P, Yepiskoposyan H, Metze S, Zamudio Orozco R, Kleinschmidt N, Mühlemann O. Nonsense-mediated mRNA decay in human cells: mechanistic insights, functions beyond quality control and the double-life of NMD factors. *Cell Mol Life Sci.* 2010;67: 677–700.
12. Kramer F, White K, Pauleikhoff D, et al. Mutations in the VMD2 gene are associated with juvenile-onset vitelliform macular dystrophy (Best disease) and adult vitelliform macular dystrophy but not age-related macular degeneration. *Eur J Hum Genet.* 2000;8:286–292.
13. Pollack K, Kreuz FR, Pillunat LE. [Best's disease with normal EOG: case report of familial macular dystrophy]. *Ophthalmologe.* 2005; 102:891–894.
14. Testa F, Rossi S, Passerini I, et al. A normal electro-oculography in a family affected by best disease with a novel spontaneous mutation of the BEST1 gene. *Br J Ophthalmol.* 2008;92:1467–1470.
15. Marmorstein LY, Wu J, McLaughlin P, et al. The light peak of the electroretinogram is dependent on voltage-gated calcium channels and antagonized by bestrophin (best-1). *J Gen Physiol.* 2006;127: 577–589.
16. Iannaccone A, Kerr NC, Kinnick TR, Calzada JI, Stone EM. Autosomal recessive best vitelliform macular dystrophy: report of a family and management of early-onset neovascular complications. *Arch Ophthalmol.* 2011;129:211–217.
17. Bitner H, Mizrahi-Meissonnier L, Griefner G, Erdinest I, Sharon D, Banin E. A homozygous frameshift mutation in BEST1 causes the classical form of Best disease in an autosomal recessive mode. *Invest Ophthalmol Vis Sci.* 2011 18;52:5332–5338.